

Electronic Supplementary Information

Readily Tunable Surface Plasmon Resonances in Gold Nanoring Arrays Fabricated Using Lateral Electrodeposition

Sunil Mehla^{*a}, Selvakannan Periasamy, Suresh K. Bhargava^{*a}

^a Centre for Advanced Materials and Industrial Chemistry, RMIT University, Melbourne, Australia

Email: suresh.bhargava@rmit.edu.au

Experimental Details

Materials: Orotemp 24 RTU (Au, cat. no. 2/0927B, Technic Inc.), Ag/AgCl (3.0 M KCl) as reference electrode and platinum wire as auxiliary electrode. The boron doped silicon wafer, AZ5214E resist and AZ400 K developer were purchased from MicroChemicals GmbH. Milli-Q water (18.2 MU cm⁻¹) was used for all synthesis, cleaning, and testing procedures.

Equipment: All lithographic patterns were designed using the KLayout software. Photolithography was performed using maskless aligner MLA 150. Kurt J. Lesker e-Beam evaporator was used for the deposition of Cr, Ni and SiO₂ thin films. Dicing of the Si wafers was performed using a Disco 321 machine with a diamond blade. The electrochemical studies were performed using a CH Instruments (CHI 760C) electrochemical analyzer in an electrochemical cell that allowed reproducible position of the working electrode, Pt wire auxiliary electrode and reference (Ag/AgCl 3.0 M KCl) electrodes and a nitrogen inlet tube for electrolyte purging (10 minutes) with nitrogen prior to electrochemistry experiments. Morphological characterization of the samples was performed using a FEI Verios SEM field emission scanning electron microscope (SEM).

Fabrication of Disc Arrays Using Maskless Photolithography: A 200 nm conducting Cr nm film was deposited on Si wafers using e-Beam evaporation. The arrays were patterned on Cr coated Si wafers using image reversal lift-off patterning. The wafers were first cleaned with

water, acetone, isopropyl alcohol and O₂ plasma. AZ5214-E resist was spin-coated on the wafers at 3000 rpm for 30 seconds followed by a soft bake at 90 °C for 90 seconds. The resist coated wafers were exposed using MLA-150 with a pattern resolution around 1 μm and an exposure power of 25 J/cm² followed by a hard bake at 120 °C for 120 seconds and UV flood exposure for 17 seconds. The obtained wafers were developed using 1:4 water/AZ400K solutions for 45 seconds and washed with water to obtain well hexagonally ordered honeycomb patterned resist film. 100 nm nickel was deposited using e-Beam evaporation and post metallization, patterns were lifted-off in acetone under sonication. After lift-off well-defined Ni disc arrays were obtained which were further coated with a SiO₂ film of 50 nm thickness using e-beam evaporation to obtain Ni-SiO₂ disc arrays.

Lateral Electrodeposition of Gold Nanoring Arrays: One-step electrodeposition using a potentiostat (CH Instruments, CHI 760C) was performed on Ni-SiO₂ disc arrays to obtain gold nanoring arrays with a conventional three-electrode system consisting of a platinum auxiliary electrode and an Ag/AgCl (3.0 M KCl) reference electrode. Commercial electrolyte Orotemp 24 RTU from Technic inc. was used as an electrolyte and electrodeposition was performed at a constant potential of -0.92V for durations of 180, 300, 600, 750 and 900 seconds to obtain GNR1, GNR2, GNR3, GNR4 and GNR5 nanoring arrays, respectively.

Reflectance Measurements: Reflectance measurements were made using the CRAIC Apollo UV-VIS-NIR spectrophotometer in the region from 200 – 2000 nm. CRAIC spectrophotometer also provided calibration standards for calibration of the equipment before use. Eight-point calibration was performed before each measurement based on the transmission spectra of holmium oxide, didymium and erbium for wavelength calibration and absorbance spectra of five calibration standards for intensity calibration. Reflectance spectrum was collected from a 50 × 50 μm² region and measurements were made from 10 different regions for Ni-SiO₂ disc arrays and gold nanoring arrays. The collected data was averaged over the 10 data points and

the reflectance plot for gold nanoring arrays was derived from the mean reflectance intensities after normalization. The reflectance data was normalized by the maximum reflectance intensity for each sample. Relative standard deviation (RSD) for measurements made from different regions of the sample was calculated to be less than 5 %.

SERS Measurements: A 10 mM solution of 4-aminothiophenol was prepared in ethanol and each sensor chip was immersed in a 2 ml aliquot from the prepared ATP solution for 15 minutes. After soaking, each chip was rinsed with water and dried under nitrogen before collection of SERS data. SERS experiments were conducted using a Perkin Elmer Raman Station 200F (785 nm laser, spot size of 50 μm) with an exposure time of 10 seconds and 5 acquisitions per data point.

FEM Modelling: A 3D electric current model of the electrode array was constructed using COMSOL Multiphysics 5.3. The model consisted of two parallel plates placed 200 μm apart, with the lower plate patterned hexagonally with conductive discs 5 μm in diameter and 100 nm high, approximating patterns fabricated experimentally. Planar surfaces of the working electrode in the intermediate region between the discs were modelled as insulating, while the top planar and lateral surfaces of the circular microelectrodes in the array were modeled as conductors with an insulating layer atop the top planar surfaces. The remaining volume between electrodes was modelled as water in place of the electrolyte solution and a bias of 1 V was applied between the two electrodes. Electric field and current density were closely aligned, as the medium exhibits real impedance and electrodeposition occurs at DC. The model was limited to a 6 x 6 array of discs with an additional 40 μm of bulk electrode and electrolyte modelled outside of the array. Minimizing the size of the model was necessary to enable computation in a timely manner, and the selected size provided homogeneous results from the center of the array (approximating a larger array), while still exhibiting fringe (edge) effects at the array boundary. Meshing was configured such that exposed lateral surfaces of discs would

have a maximum distance between elements of 200 nm, to provide good resolution in the regions where growth was observed.

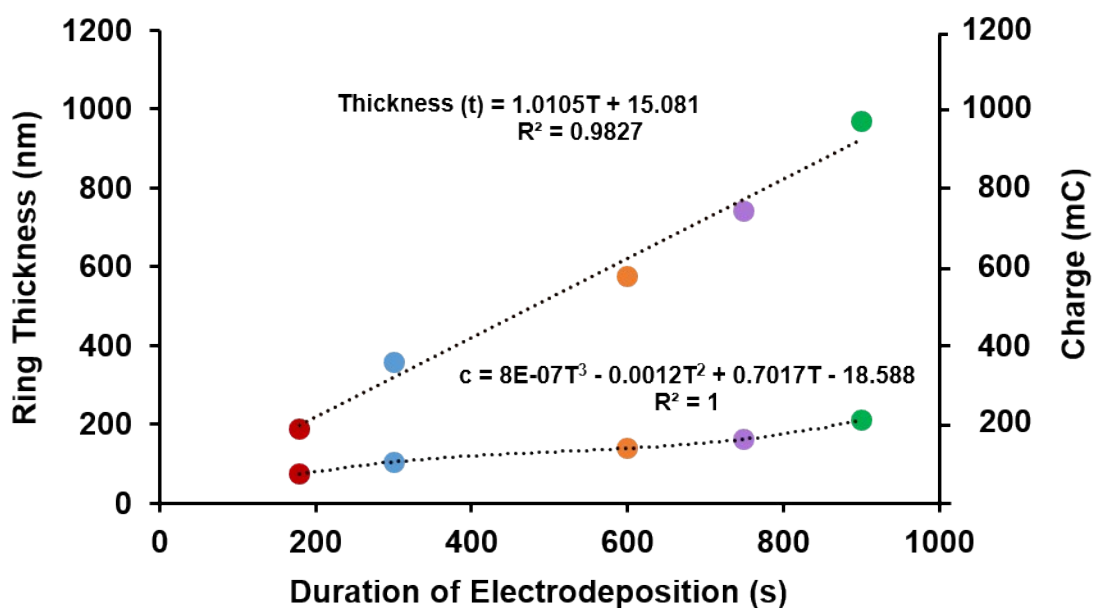


Fig. S1 Variation of ring thickness (t) and charge (c) passed through the solution with duration of electrodeposition (T). A linear correlation was identified between the ring thickness and duration of electrodeposition whereas a third order correlation was identified between the charge passed through the solution and duration of electrodeposition.

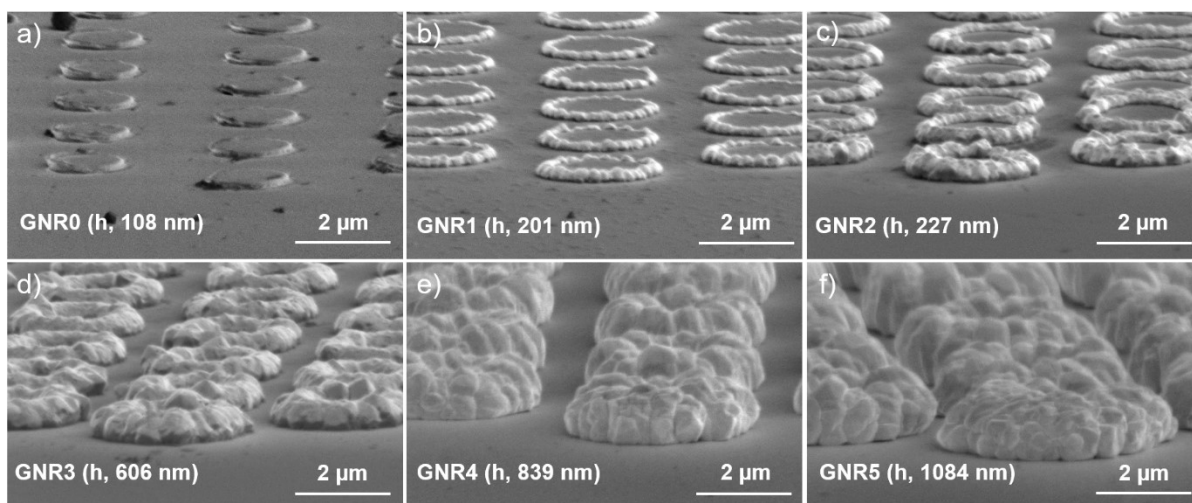


Fig. S2. Tilted SEM images for fabricated samples indicating the rough surface of the electrodeposited gold rings and used height measurements; a) Ni-SiO₂ disc array of height 108 nm; b) gold nanoring array of height 201 nm (GNR1); c) gold nanoring array of height 227 nm (GNR2); d) gold nanoring array of height 606 nm (GNR3); e) gold nanoring array of height 839 nm (GNR4); and f) gold nanoring array of height 1084 nm (GNR5).

Evolution of the Internal and External Diameter of Gold nanoring arrays with Electrodeposition Time

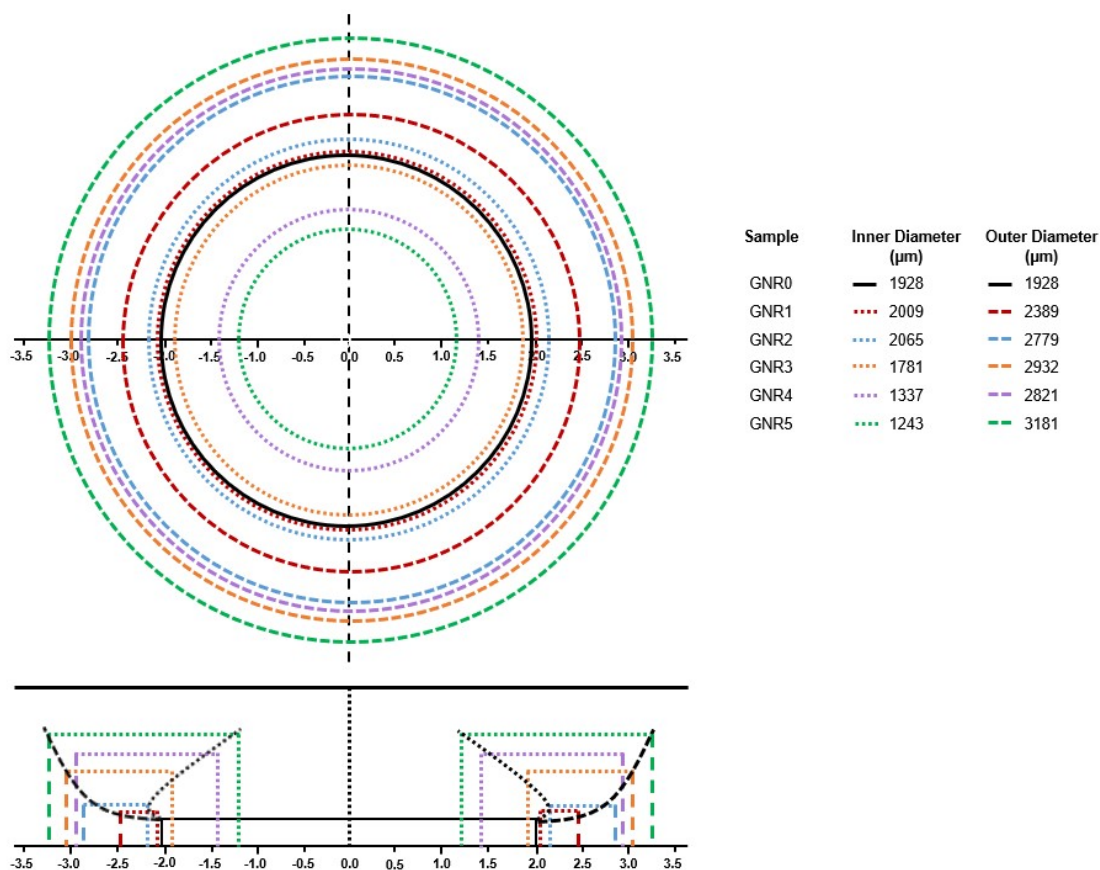


Fig. S3. An illustration depicting the growth of gold nanorings on the lateral surfaces of Ni-SiO₂ disc arrays (black). Initially both the inner surface and outer surface of gold rings grow outwards away from the lateral surfaces as evident from GNR1 and GNR2. Beyond a certain height the inner surface of gold rings changes the direction of growth and curl inwards toward the center of the Ni-SiO₂ as evident from the inner and outer diameters for GNR3, GNR4 and GNR5.

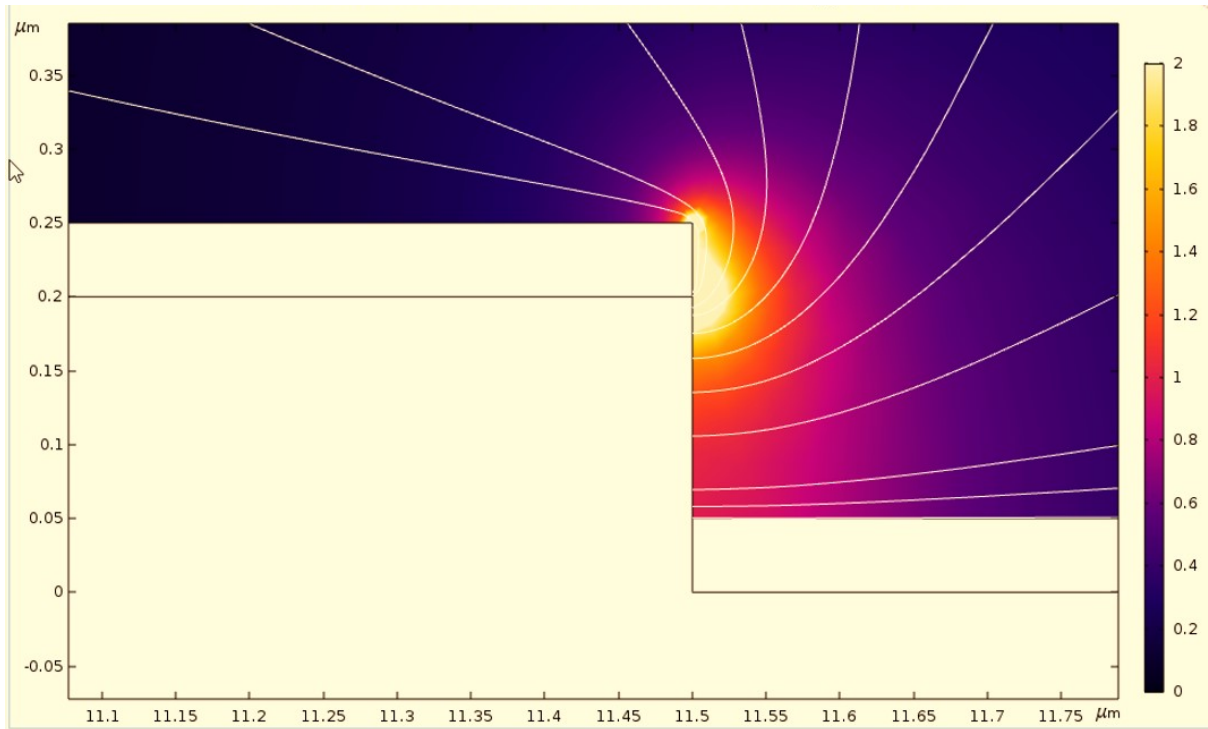


Fig. S4 FEM simulations for normalized electric field magnitude and electric field lines for a single 2 μm Ni-SiO₂ disc. The reduction of gold ions on the lateral surfaces and growth of gold rings tends to follow the electric field lines originating perpendicular to the lateral surfaces but bending upwards towards the counter electrode and curling inwards towards the center of the disc. A higher intensity of electric field at the edge of the disc due to the fringe effect can also be seen from the FEM simulations.